

Entanglement structure of the two-channel Kondo model

Bedoor Alkurtass,^{1,2} Abolfazl Bayat,¹ Ian Affleck,³ Sougato Bose,¹
Henrik Johannesson,⁴ Pasquale Sodano,^{5,6} Erik S. Sørensen,⁷ and Karyn Le Hur⁸

¹*Department of Physics and Astronomy, University College London, Gower Street, London WC1E 6BT, UK*

²*Department of Physics and Astronomy, King Saud University, Riyadh 11451, Saudi Arabia*

³*Department of Physics and Astronomy, University of British Columbia, Vancouver, British Columbia V6T 1Z1, Canada*

⁴*Department of Physics, University of Gothenburg, SE 412 96 Gothenburg, Sweden*

⁵*International Institute of Physics, Universidade Federal do Rio Grande do Norte, 59078-400 Natal-RN, Brazil*

⁶*Departamento de Física Teórica e Experimental, Universidade Federal do Rio Grande do Norte, 59072-970 Natal-RN, Brazil*

⁷*Department of Physics and Astronomy, McMaster University, Hamilton, Ontario L8S 4M1, Canada*

⁸*Centre de Physique Théorique, Ecole Polytechnique, CNRS, Université Paris-Saclay, 91128 Palaiseau Cedex, France*

Two electronic channels competing to screen a single impurity spin, as in the two-channel Kondo model, are expected to generate a ground state with nontrivial entanglement structure. We exploit a spin-chain representation of the two-channel Kondo model to probe the ground-state block entropy, negativity, tangle, and Schmidt gap, using a density matrix renormalization group approach. In the presence of symmetric coupling to the two channels we confirm field-theory predictions for the boundary entropy difference, $\ln(g_{UV}/g_{IR}) = \ln(2)/2$, between the ultraviolet and infrared limits and the leading $\ln(x)/x$ impurity correction to the block entropy. The impurity entanglement, S_{imp} , is shown to scale with the characteristic length $\xi_{2\text{CK}}$. We show that both the Schmidt gap and the entanglement of the impurity with one of the channels – as measured by the negativity – faithfully serve as order parameters for the impurity quantum phase transition appearing as a function of channel asymmetry, allowing for explicit determination of critical exponents, $\nu \approx 2$ and $\beta \approx 0.2$. Remarkably, we find the emergence of tripartite entanglement only in the vicinity of the critical channel-symmetric point.

Introduction. - The Kondo effect is one of the most intriguing effects in quantum many-body physics. At low temperatures, a localized magnetic impurity is screened by the conduction electrons leading to the formation of many-body entanglement. A generalization of the Kondo model was introduced by Nozières and Blandin [1], where another channel of electrons is also coupled to the impurity. This is the well-known two-channel Kondo (2CK) model, for which various results were obtained using Bethe ansatz [2–4], conformal field theory [5, 6] (CFT), bosonization [7–9] and entanglement of formation [10]. This model is very different from the one-channel Kondo (1CK) model as the two channels compete to screen the spin-1/2 impurity, leading to an “overscreened” residual spin interacting with the electrons [5]. This leads to non-trivial properties including a residual zero-temperature impurity entropy and a logarithmic behavior of magnetic susceptibility and specific heat. However, channel symmetry is crucial; even the smallest asymmetry leads to screening of the impurity by the channel with the stronger coupling [1], and as the channel asymmetry is varied, an impurity quantum phase transition (IQPT) occurs at the symmetric point, corresponding to the 2CK model.

Intensive research has been carried out to investigate the thermodynamics and the transport properties of the 2CK model [1–3, 5–9, 11–25]. Experimentally, signatures of the 2CK model have been observed in mesoscopic structures [26–29]. Still, the real-space entanglement structure and the imprints of the two distinct length scales $\xi_{2\text{CK}} \sim u/T_{2\text{CK}}$ and $\xi^* \sim u/T^*$ with u the spin velocity – implied by the known crossover energy scales $T_{2\text{CK}}$ (2CK temperature) and T^* (critical crossover in the channel-asymmetric case) [5, 23] – have not yet been unraveled. A way forward is to use a spin-chain

representation of the 2CK model [11, 12], which allows for efficient Density Matrix Renormalization Group (DMRG) computations [30–34] ($m = 100 - 1024$ states kept) to uncover the ground state entanglement properties.

In this letter, we show how the implementation of this scheme allows for a detailed study of the entanglement in the 2CK ground state and the IQPT between the two channel-asymmetric 1CK phases. Specifically, we present results for the impurity entanglement entropy [30, 31], the negativity [35, 36], the Schmidt gap [37, 38], and the tripartite entanglement [39, 40]. At the channel-symmetric 2CK point we show that $\xi_{2\text{CK}}$ can be interpreted as a dynamically generated cut-off length by demonstrating scaling of the impurity entanglement entropy. A detailed analysis allows us to extract the two-channel boundary entropy difference $\ln(g_{UV}/g_{IR}) = \ln(2)/2$, between the ultraviolet and infrared limits [41], as well as the leading correction $\ln(x)/x$, for block sizes $x \gg \xi_{2\text{CK}}$ [42]. In addition, we show that the negativity and the Schmidt gap act as order parameters for the IQPT, enabling us to predict, via finite-size scaling, the pertinent critical exponents. Finally, we compute the tangle [39, 40] and show that tripartite entanglement emerges *only* in the vicinity of the critical point.

Spin-chain representation. - We consider two open Heisenberg chains coupled to a single spin-1/2 impurity as shown in Fig. 1(a). The open chain Hamiltonian is given by

$$H_{\text{OBC}} = \sum_{m=L,R} \left[J'_m (J_1 \sigma^0 \cdot \sigma_m^1 + J_2 \sigma^0 \cdot \sigma_m^2) + J_1 \sum_{l=1}^{N_m-1} \sigma_m^l \cdot \sigma_m^{l+1} + J_2 \sum_{l=1}^{N_m-2} \sigma_m^l \cdot \sigma_m^{l+2} \right], \quad (1)$$

where σ^0 and σ_m^l represent the vector of Pauli matrices for

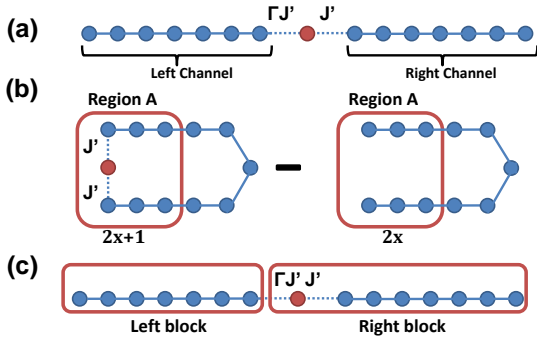


FIG. 1. (Color online) (a) Kondo spin chain with a spin-1/2 impurity coupled to its left and right channels by $\Gamma J'$ and J' , respectively. For $\Gamma = 1$ the impurity is screened by both channels representing the 2CK model while for $\Gamma \neq 1$ 1CK physics emerges. (b) The impurity entropy S_{imp} is computed as the difference between the entropy of region A with and without the impurity. (c) Partitioning of the system for computing the Schmidt gap.

the impurity spin and the spin at site l in channel m , respectively, and N_m is the number of spins in chain m making the total number of spins $N = N_L + N_R + 1$. We choose the nearest-neighbor coupling J_1 to be unity and the next-nearest-neighbor coupling $J_2 = J_2^c$ (with $J_2^c = 0.2412J_1$) so as to remove marginal coupling effects [34, 43]. In this work, we set the Kondo coupling $J'_L = \Gamma J'$ and $J'_R = J'$, with $\Gamma = J'_L/J'_R$ keeping $J'_m < 1$. The Hamiltonian (1) has been introduced in Ref. [11, 12] as a representation of the spin sector of the 2CK model when $\Gamma = 1$. For further justifications, see the Supplemental Material. For any $\Gamma \neq 1$ 1CK physics emerges. For the case of $\Gamma = 1$, we also use a periodic chain, as shown on the left side of the Fig. 1(b), by adding the following terms:

$$H_{PBC} = H_{OBC} + J_1 \sigma_L^{N_L} \cdot \sigma_R^{N_R} + J' J_2 \sigma_L^1 \cdot \sigma_R^1 + J_2 (\sigma_L^{N_L} \cdot \sigma_R^{N_R-1} + \sigma_L^{N_L-1} \cdot \sigma_R^{N_R}). \quad (2)$$

Again $N = N_L + N_R + 1$, and at $J' = 1$ we obtain a uniform periodic chain which presents significant advantages [44]. In the limit of $N \rightarrow \infty$ the two boundary conditions are equivalent. For H_{OBC} the parity of $N_L = N_R$ is crucial [45] but here we only study $N_L = N_R$ odd, however, for H_{PBC} it is the parity of N that matters [45] and we only study N even ($N_L = N_R \pm 1$) which makes the parity effects compatible for H_{OBC} and H_{PBC} .

Impurity entanglement entropy.— We first study the channel-symmetric case, $\Gamma = 1$, with ξ_{2CK} being the only relevant length scale in the problem. We consider the von Neumann entropy, $S_A(J', x, N) = -\text{Tr} \rho_A \log \rho_A$ with ρ_A the reduced density matrix of a region A which includes the impurity spin and x spins on either side of it. N is the total number of spins in the system, including the impurity. We consider an even periodic system, using H_{PBC} as shown in Fig. 1(b). This boundary condition should not affect our results as long as $x \ll N/2$ [44]. Similar to the single-channel case [30, 31] the entanglement entropy behaves very differently in the two limits $x \ll \xi_{2CK}$ and $x \gg \xi_{2CK}$, with $\xi_{2CK} \sim e^{aJ'}$ growing exponentially as $J' \rightarrow 0$ (for some constant a). In what follows we shall show how to pinpoint the impurity contribution, S_{imp} , to the von

Neumann entropy. By doing so, we provide a direct “quantum probe” of the boundary entropy predicted by CFT [41], with no reference to the thermodynamic entropy.

Let’s first consider the $N \rightarrow \infty$ limit. When $J' = 1$, we simply have a uniform periodic chain with region A consisting of $2x + 1$ sites. Then, using the fact that the central charge $c = 1$, the entanglement entropy for region A of a periodic chain is predicted to be, from CFT [46]

$$S_A(J' = 1, x, N) = \frac{1}{3} \ln(2x + 1) + s_1 \quad (3)$$

for a non-universal constant s_1 . For *finite* but large N even, we expect the limit of $J' \rightarrow 0^+$, $x \ll N$ (which is different from the case where the impurity is absent) to give:

$$S_A(J' \rightarrow 0^+, x, N) = S_A(x, N - 1) + \ln 2 \quad (4)$$

where $S_A(x, N - 1)$ represents the entropy of region A when the impurity is absent but the region still consists of x spins from each channel (so the total length is $N - 1$) as shown on the right side of Fig. 1(b). The additional $\ln 2$ entanglement entropy in Eq. (4) is the impurity contribution and can be understood by observing that a spin chain with an even number of sites has a spin zero ground state for any $J' > 0$ no matter how small. In a valence bond picture of the N even ground state there will always be an (impurity) valence bond (IVB) connecting the impurity spin to another spin in the system, although the IVB becomes very long in the small J' limit [30, 31]. Intuitively, this long IVB adds an extra $\ln 2$ to $S_A(J' \rightarrow 0^+, x, N)$. The interesting case of N odd will be considered elsewhere [45].

In the absence of an impurity, as long as $x \ll N/2$, the entropy of region A is the sum of the entropy of two equal blocks at either end of an open chain as shown in the right part of Fig. 1(b). In this case the open boundaries induce an alternating term in the entanglement entropy [47] and we therefore only focus on the uniform part, S^u finding [46, 48]

$$S_A^u(x, N - 1) = 2 \left[\frac{1}{6} \ln(2x) + \frac{s_1}{2} + \ln g \right], \quad (5)$$

where s_1 is the same non-universal constant appearing in Eq. (3) and $\ln g$ is a universal term arising from a non-integer “ground-state degeneracy”, g [41].

The difference between the two entropies of the two extreme regimes will be

$$S_A(J' = 1, x, N) - S_A^u(J' \rightarrow 0^+, x, N) = -2 \ln g - \ln 2 + O(1/x). \quad (6)$$

Using the mapping of the spin-chain system onto the 2CK model, we associate $J' \rightarrow 0^+$ with the weak coupling ultraviolet fixed point and $J' \rightarrow 1$ with the infrared fixed point. Hence we expect

$$S_A(J' = 1, x, N) - S_A^u(J' \rightarrow 0^+, x, N) = \ln g_{IR} - \ln g_{UV}, \quad (7)$$

where $\ln g_{UV}$ and $\ln g_{IR}$ are the boundary entropies for the ultraviolet and infrared fixed points. Hence, it follows that the degeneracies of the 2CK model and the open chain *must be*

related as $g_{UV}/g_{IR} = 2g^2$. While $g_{UV} = 2$, corresponding to the decoupled impurity spin, g_{IR} has the non-trivial value of $\sqrt{2}$. On the other hand, g was predicted, using field theory arguments for the open spin chain to have the value $2^{-1/4}$ [11, 12, 49] validating the relation $g_{UV}/g_{IR} = 2g^2 = \sqrt{2}$. This constitutes a highly non-trivial check of the spin-chain representation of the 2CK model. We confirm the result $g = 2^{-1/4}$ by extracting s_1 from DMRG results for the entanglement entropy for an even periodic chain, finding $s_1 = 0.743743$. We then fit S_A^u for a single open chain of length N to the finite N generalisation of Eq. (5)

$$S_A^u(x, N) = 2 \left[\frac{1}{6} \ln[(2N/\pi) \sin(\pi x/N)] + \frac{s_1}{2} + \ln g \right] + \frac{\alpha}{N} [2 + \pi(1 - 2x/N) \cot(\pi x/N)]. \quad (8)$$

Here the last term is a correction, behaving as α/x in the $N \rightarrow \infty$ limit, calculated in [30, 31, 45] where α is a non-universal parameter. S_A^u is extracted using a 7-point formula [30, 31, 45]. With s_1 known, this then determines $\ln g = -0.17328$, in excellent agreement with $\ln(2^{-1/4}) = -0.1732867 \dots$

We now show that $\ln(g_{UV}/g_{IR})$ enters as part of the limiting behavior of the impurity entanglement entropy allowing us to numerically estimate this boundary entropy difference. We begin by considering the behaviour of S_A for intermediate values of J' . Most notably, an alternating term appear in S_A for any $J' \neq 1$ [45]. Hence, by subtracting off the entropy with the impurity absent [30, 31], as shown in Fig. 1(b), we define the impurity entanglement entropy using the *uniform part* as

$$S_{\text{imp}}(J', x, N) = S_A^u(J', x, N) - S_A^u(x, N - 1). \quad (9)$$

The hallmark feature of the characteristic length $\xi_{2\text{CK}} \sim u/T_{2\text{CK}}$ is that S_{imp} is a *universal* scaling function of the two variables x/N and $x/\xi_{2\text{CK}}$. Again, the parity of N also plays a crucial role [45] but here we only focus on N even. If we fix $x/N = 1/10$, S_{imp} should then be a function of the single variable $x/\xi_{2\text{CK}}$. However, as evident from Eq. (8) the term proportional to α in $S_A^u(x, N - 1)$ gives rise to corrections to scaling disappearing as $N \rightarrow \infty$ with x/N and $x/\xi_{2\text{CK}}$ held fixed. For clarity, we subtract these corrections from S_{imp} obtaining $S_{\text{imp}}^{\text{sub}}$. In Fig. 2(a) we demonstrate the scaling by collapsing data for many values of J' and N with fixed x/N onto a single curve by appropriately selecting $\xi_{2\text{CK}}(J')$. The expected $\xi_{2\text{CK}} \sim e^{a/J'}$ behavior is also confirmed (inset of Fig. 2(a)). We see that an excellent data collapse appears for a range of J' and the data approaches fairly closely to $\ln(2)/2 = 0.3465$ at large $x/\xi_{2\text{CK}}$. This limit corresponds to $J' \rightarrow 1$ and using Eq. (4) and (7) we have $S_{\text{imp}}(J' \rightarrow 1) = \ln(2) - \ln(g_{UV}/g_{IR}) = \ln(2)/2$ so we can conclude [44]:

$$\ln(g_{UV}/g_{IR}) \simeq \ln(2)/2, \quad g_{UV}/g_{IR} \simeq \sqrt{2} \quad (10)$$

providing a firm confirmation of the CFT predictions.

For $x \gg \xi_{2\text{CK}}$ at $N \rightarrow \infty$ we are close to the infrared fixed point. The leading irrelevant operator has dimension $3/2$ [5] and is expected to lead to corrections to the leading $\ln(2)/2$

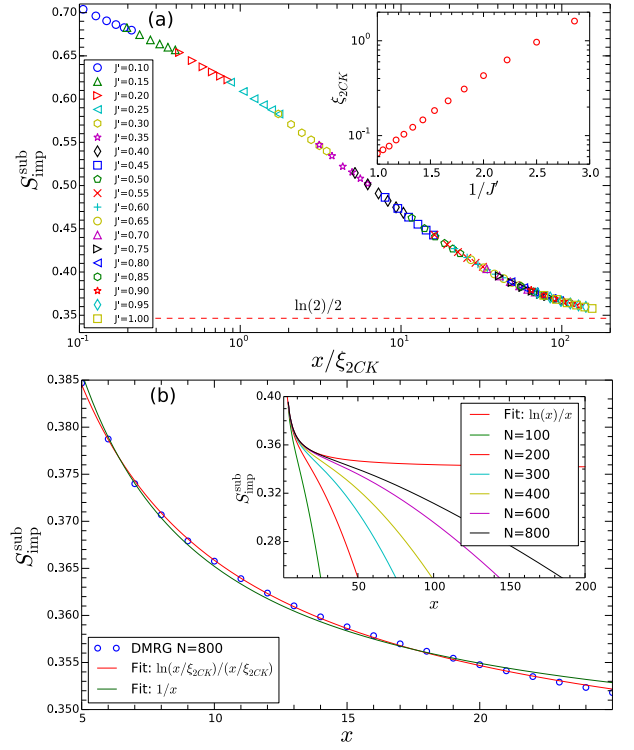


FIG. 2. (Color online) (a) Scaling of $S_{\text{imp}}^{\text{sub}}(x/\xi_{2\text{CK}}(J'))$ for fixed $x/N = 1/10$ (N even). At $J' = 0.9$, $\xi_{2\text{CK}}(J')$ is arbitrarily fixed at 0.07747 to coincide with the estimate from panel b. Inset: $\xi_{2\text{CK}}(J')$ as a function of $1/J'$. (b) DMRG results for $S_{\text{imp}}^{\text{sub}}(x; J' = 0.9, N = 800)$. For $\xi_{2\text{CK}}(J') \ll x \ll N/2$ $S_{\text{imp}}^{\text{sub}}$ can be fit to the form $A \ln(x/\xi_{2\text{CK}})/(x/\xi_{2\text{CK}}) + B$ (red line) with $\xi_{2\text{CK}}(J' = 0.9) = 0.07747$, $A = 0.69$ and $B = 0.34 \sim \ln(2)/2$ significantly better than to $\sim 1/x$ (green line). Inset: Convergence to the limiting form at $x \ll N/2$ with N .

behavior of S_{imp} that in second-order perturbation theory are of the form $\delta S_{\text{imp}} \propto \ln(x)/x$ [42], valid in the regime $\xi_{2\text{CK}} \ll x \ll N/2$. Numerically we can confirm this by studying $S_{\text{imp}}^{\text{sub}}$ for $J' \sim 1$ where $\xi_{2\text{CK}}$ is small. This is shown in Fig. 2(b) for $J' = 0.9$ where a fit to $\ln(x)/x$ correction is statistically superior to a simpler $1/x$ form over a significant range of x .

Negativity as an order parameter.— Several entanglement measures have been used to detect quantum phase transitions [37, 38, 50–54]. Here, we propose the negativity [35, 36] as an order parameter for the IQPT, with Γ as control parameter. For any bipartite density matrix ρ_{AB} the negativity, as an entanglement measure, is defined as $E_{A,B} = -1 + \sum_k |\eta_k|$, where η_k 's are the eigenvalues of the matrix $\rho_{AB}^{T_A}$, where T_A stands for partial transposition with respect to subsystem A [44]. In this section, and through the remainder of the paper we use H_{OBC} , with $N_L = N_R$ odd. In Fig. 3(a) we plot the negativity between impurity and right channel, $E_{0,R}$, versus Γ . It is expected that the ground state is overscreened only at $\Gamma = 1$ where the impurity is entangled with both channels. For any $\Gamma \neq 1$ in the thermodynamic limit, the impurity is screened only by the channel with the strongest coupling to the impurity, resulting in a fully screened 1CK phase. Indeed, the behavior of the negativity is consistent; $E_{0,R}$ goes from 1 to 0 around the critical point.

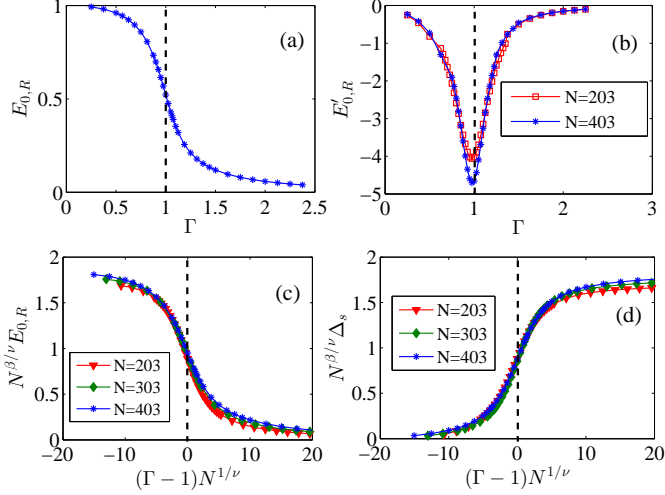


FIG. 3. (Color online) (a) Negativity between the impurity and the right channel (i.e. $E_{0,R}$) versus Γ for $N = 403$ and $J' = 0.4$. (b) Derivative of $E_{0,R}$ with respect to Γ for different system sizes. (c) Finite size scaling of $E_{0,R}$. (d) Finite-size scaling of the Schmidt gap.

The thermodynamic behavior can be explored by studying the derivative of the negativity with respect to Γ , namely $E'_{0,R}$, shown in Fig. 3(b). As the figure shows, the derivative dips at the critical point with the dip sharpening as N increases. This suggests that, as $N \rightarrow \infty$, $E'_{0,R}$ diverges at the critical point, implying that the 2CK ground state is destroyed and 1CK physics is emerging.

The interpretation of the negativity as an order parameter can be justified by a finite-size scaling analysis [55]. An order parameter scales as $|\Gamma - 1|^\beta$ in the vicinity of the critical point and the correlation length as $|\Gamma - 1|^{-\nu}$, where β and ν are critical exponents. The role of a correlation length is here taken by the critical crossover scale ξ^* at which the renormalization-group flow of the channel-asymmetric model crosses over from the unstable overscreened fixed point to the fully screened Kondo fixed point [5, 23]. Finite-size scaling [55] implies that

$$E_{0,R} = N^{-\beta/\nu} F(|\Gamma - 1| N^{1/\nu}), \quad (11)$$

with F a scaling function. In Fig. 3(c), we plot $N^{\beta/\nu} E_{0,R}$ as a function of $(\Gamma - 1) N^{1/\nu}$. When $\nu = 2 \pm 0.05$ and $\beta = 0.2 \pm 0.02$, curves for different N collapse to a single curve. The value of $\nu \approx 2$ matches CFT [5] and bosonization results [19], verifying that the negativity behaves as an order parameter. Here $\nu = 1/d$, with d the scaling dimension of the relevant operator that appears in the Hamiltonian when parity symmetry is broken.

Schmidt gap.- Another key quantity, related to the entanglement spectrum, is the Schmidt gap Δ_S . Given a bipartitioning of the system, it is defined by $\Delta_S = \lambda_1 - \lambda_2$, where $\lambda_1 \geq \lambda_2$ are the two largest eigenvalues of the reduced density matrix of any of the two subsystems. It was recently shown that the Schmidt gap can serve as an order parameter across quantum phase transitions [37, 38]. For the 2CK model close to $\Gamma = 1$, and choosing a bipartition as shown in Fig. 1(c) for two com-

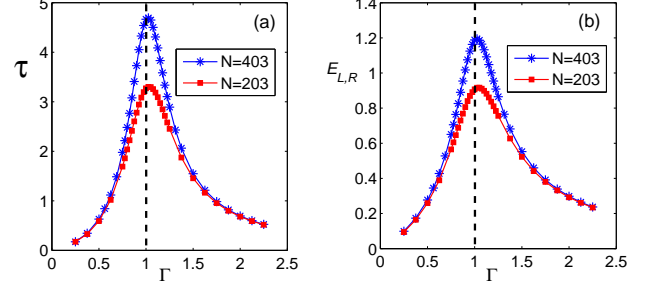


FIG. 4. (Color online) (a) The tripartite entanglement indicator τ versus Γ . (b) Entanglement between the two channels versus Γ . In both panels $J' = 0.4$.

plementary left and right blocks, the Schmidt gap is found to obey finite-size scaling with the same critical exponents as the negativity. Fig. 3(d) shows the Schmidt gap data collapse for three different system sizes, confirming it as an alternative order parameter to the negativity in the 2CK model.

Tripartite entanglement.- Changing from 1CK to 2CK physics changes the entanglement structure fundamentally. Inspired by tangle [39] and its generalization for negativity [40], as tripartite entanglement measures for qubits, we introduce a tripartite entanglement indicator as

$$\tau = (\pi_0 + \pi_L + \pi_R)/3 \quad (12)$$

in which

$$\pi_0 = E_{0,LR}^2 - E_{0,L}^2 - E_{0,R}^2, \quad \pi_m = E_{m,0\bar{m}}^2 - E_{m,0}^2 - E_{m,\bar{m}}^2,$$

where $m = L, R$ and $\bar{m} = R, L$ represent opposite channels, $E_{0,LR} = 1$ is the negativity of the impurity with the rest of the system, $E_{0,m} = E_{m,0}$ is the negativity between the impurity and channel m , and $E_{m,\bar{m}}$ is the negativity between the two channels. For systems with *odd* length leads each channel effectively behaves like a spin-1/2 system and our tripartite entanglement indicator τ becomes a natural generalization of the tangle defined for three qubits [40]. In Fig. 4(a) we plot τ versus Γ for systems with odd length leads. τ clearly peaks at the critical point with the peak becoming more pronounced with increasing length, suggesting its divergence with N . The emergence of tripartite entanglement is therefore related to the overscreening at the critical point where the two channels become highly entangled. In Fig. 4(b), we plot the negativity between the two channels, $E_{L,R}$, versus Γ . As the figure shows, $E_{L,R}$ is maximal at $\Gamma = 1$, likely diverging with N .

Conclusions.- Employing high-precision DMRG computations, we have studied the ground state entanglement of the 2CK model, allowing us to uncover the fractional ground state degeneracy predicted by CFT. The existence of the characteristic length scale ξ_{2CK} is established through a scaling analysis of S_{imp} . The IQPT appearing as a function of channel-asymmetry and its exponents is detected using both the negativity and the Schmidt gap as order parameters. Furthermore, the tangle is used to show that tripartite entanglement emerges only in the vicinity of the critical point.

Acknowledgements.- The authors would like to thank E. Eriksson and N. Laflorencie for valuable discussions and acknowledge the use of the UCL Legion High Performance Computing Facility (Legion@UCL), and associated support services, in the completion of this work. Part of the calculations was made possible by the facilities of the Shared Hierarchical Academic Research Computing Network (SHARCNET:www.sharcnet.ca) and Compute/Calcul Canada and some of the calculations were performed using the ITensor library [56]. BA is funded by King Saud University. AB and SB are supported by the EPSRC grant EP/K004077/1. IA is supported by NSERC Discovery Grant 36318-2009 and by CIFAR. ESS is supported by NSERC Discovery Grant. SB also acknowledges support of the ERC grant PACOMANEDIA and EPSRC grant EP/J007137/1. HJ acknowledges support from the Swedish Research Council and STINT. PS thanks the Ministry of Science, Technology and Innovation of Brazil, MCTI and UFRN/MEC for financial support and CNPq for granting a "Bolsa de Produtividade em Pesquisa". KLH also acknowledges the CIFAR in Canada and KITP for hospitality.

-
- [1] P. Nozières and A. Blandin, *Journal de Physique* **41**, 193 (1980).
 [2] N. Andrei and C. Destri, *Phys. Rev. Lett.* **52**, 364 (1984).
 [3] A. M. Tselvick and P. B. Wiegmann, *Z. Phys. B Cond. Mat.* **54**, 201 (1984).
 [4] A. M. Tselvick, *J. Phys. C* **18**, 159 (1985).
 [5] I. Affleck and A. W. W. Ludwig, *Nucl. Phys. B* **360**, 641 (1991).
 [6] I. Affleck and A. W. W. Ludwig, *Phys. Rev. B* **48**, 7297 (1993).
 [7] V. Emery and S. Kivelson, *Phys. Rev. B* **46**, 10812 (1992).
 [8] D. G. Clarke, T. Giamarchi and B. Shraiman, *Phys. Rev. B* **48**, 7070 (1993).
 [9] A. Sengupta and A. Georges, *Phys. Rev. B* **49**, 10020(R) (1994).
 [10] S.-S. B. Lee, J. Park, and H.-S. Sim, *Phys. Rev. Lett.* **114**, 057203 (2015).
 [11] S. Eggert and I. Affleck, *Phys. Rev. B* **46**, 10866 (1992).
 [12] I. Affleck in *Correlation Effects in Low Dimensional Systems* (ed. A. Okiji and N. Kawakami, Springer-Verlag, Berlin, 1994), p 82. arXiv:cond-mat/9311054.
 [13] S. Eggert, D. P. Gustafsson, and S. Rommer, *Phys. Rev. Lett.* **86**, 516 (2001).
 [14] D. M. Cragg, P. Loyd, and P. Nozières, *J. Phys. C* **13**, 803 (1980).
 [15] P. Sacramento and P. Schlottmann, *Phys. Rev. B* **43**, 13294 (1991).
 [16] I. Affleck, A. W. W. Ludwig, H. -B. Pang, and D. L. Cox, *Phys. Rev. B* **45**, 7918 (1992).
 [17] J. Gan, N. Andrei, and P. Coleman, *Phys. Rev. Lett.* **70**, 686 (1993).
 [18] N. Andrei and A. Jerez, *Phys. Rev. Lett.* **74**, 4507 (1995).
 [19] M. Fabrizio, A. O. Gogolin, and P. Nozières, *Phys. Rev. Lett.* **74**, 4503 (1995).
 [20] G. Zaránd and J. von Delft, *Phys. Rev. B* **61**, 6918 (2000).
 [21] S. Yotsuhashi and H. Maebashi, *J. Phys. Soc. Jpn.* **71**, 1705 (2002).
 [22] A. I. Tóth and G. Zaránd, *Phys. Rev. B* **78**, 165130 (2008).
 [23] A. K. Mitchell, M. Becker, and R. Bulla, *Phys. Rev. B* **84**, 115120 (2011).
 [24] A. K. Mitchell and E. Sela, *Phys. Rev. B* **85**, 235127 (2012).
 [25] C. Mora and K. Le Hur, *Phys. Rev. B* **88**, 241302 (2013).
 [26] R. M. Potok, I. G. Rau, H. Shtrikman, Y. Oreg and D. Goldhaber-Gordon, *Nature* **446**, 167-171 (2007).
 [27] H. T. Mebrahtu, I. V. Borzenets, H. Zheng, Y. V. Bomze, A. I. Smirnov, S. Florens, H. U. Baranger, G. Finkelstein, *Nat. Phys.* **9**, 732 (2013).
 [28] Z. Iftikhar, S. Jezouin, A. Anthore, U. Gennser, F. D. Parmentier, A. Cavanna and F. Pierre, *Nature* **526**, 233 (2015).
 [29] A. J. Keller, L. Peters, C. P. Moca, I. Weymann, D. Mahalu, V. Umansky, G. Zaránd, and D. Goldhaber-Gordon, *Nature* **526**, 237 (2015).
 [30] E. S. Sørensen, N. Laflorencie, M.-S. Chang, and I. Affleck, *J. Stat. Mech.* L01001 (2007).
 [31] E. S. Sørensen, M.-S. Chang, N. Laflorencie, and I. Affleck, *J. Stat. Mech.* P08003 (2007).
 [32] I. Affleck, N. Laflorencie, and E. S. Sørensen, *J. Phys. A.* **42**, 504009 (2009).
 [33] A. Bayat, P. Sodano, and S. Bose, *Phys. Rev. B* **81**, 064429 (2010).
 [34] A. Bayat, S. Bose, P. Sodano, and H. Johannesson, *Phys. Rev. Lett.* **109**, 066403 (2012).
 [35] J. Lee, M. S. Kim, Y. J. Park, and S. Lee, *J. Mod. Opt.* **47**, 2151 (2000).
 [36] G. Vidal and R. F. Werner, *Phys. Rev. A* **65**, 032314 (2002).
 [37] G. De Chiara, L. Lepori, M. Lewenstein and A. Sanpera, *Phys. Rev. Lett.* **109**, 237208 (2012).
 [38] A. Bayat, H. Johannesson, S. Bose and P. Sodano, *Nat. Commun.* **5**, 3784 (2014).
 [39] V. Coffman, J. Kundu, and W. K. Wootters, *Phys. Rev. A* **61**, 052306 (2000).
 [40] Y.-C. Ou, H. Fan, *Phys. Rev. A* **75**, 062308 (2007).
 [41] I. Affleck and A. W. W. Ludwig, *Phys. Rev. Lett.* **67**, 161 (1991).
 [42] E. Eriksson and H. Johannesson, *Phys. Rev. B* **84**, 041107(R) (2011).
 [43] N. Laflorencie, E. S. Sørensen, and I. Affleck, *J. Stat. Mech.* P02007 (2008).
 [44] See Supplemental Material.
 [45] I. Affleck, B. Alkurtass, A. Bayat, S. Bose, H. Johannesson, K. Le Hur, P. Sodano, E. S. Sørensen to be published.
 [46] C. Holzhey, F. Larsen, and F. Wilczek, *Nucl. Phys. B* **424** 44 (1994); P. Calabrese and J. Cardy, *J. Stat. Mech.* 0406: P06002 (2004).
 [47] N. Laflorencie, E. S. Sørensen, M.-S. Chang and I. Affleck, *Phys. Rev. Lett.* **96**, 100603 (2006).
 [48] H. Q. Zhou, T. Barthel, J. O. Fjærestad and U. Schollwöck, *Phys. Rev. A* **74** 050305 (2006).
 [49] M. Oshikawa and I. Affleck, *Nucl. Phys. B* **495**, 533 (1997).
 [50] L. Amico, R. Fazio, A. Osterloh, and V. Vedral, *Rev. Mod. Phys.* **80**, 517 (2008).
 [51] K. Le Hur, Ph. Doucet-Beaupré and W. Hofstetter, *Phys. Rev. Lett.* **99**, 126801 (2007); A. Kopp and K. Le Hur, *Phys. Rev. Lett.* **98**, 220401 (2007).
 [52] K. Le Hur, *Annals of Physics* **323**, 2208 (2008).
 [53] S. Rachel, N. Laflorencie, H. F. Song and K. Le Hur, *Phys. Rev. Lett.* **108**, 116401 (2012).
 [54] H. F. Song, S. Rachel, C. Flindt, I. Klich, N. Laflorencie, K. Le Hur, *Phys. Rev. B* **85**, 035409 (2012).
 [55] M. N. Barber, in *Phase Transitions and Critical Phenomena Vol. 8*, eds. C. Domb and J. L. Lebowitz, p. 145-477 (Academic Press, London, 1983).
 [56] <http://itensor.org/>
 [57] I. Affleck, *Field Theory Methods and Quantum Critical Phenomena*

Supplemental Material

1. Review of negativity as an entanglement measure

In a bipartite system AB , quantification of entanglement between the two subsystems has been intensively studied in the last decade. When the density matrix of the overall system ρ_{AB} is pure then the von Neumann entropy of the subsystem, namely $S(\rho_A) = -\text{Tr}\{\rho_A \log \rho_A\}$ where ρ_A is the reduced density matrix of the subsystem A , is a unique measure of entanglement and all other measures are monotonic functions of the von Neumann entropy. At variance, when the overall state ρ_{AB} is mixed the von Neumann entropy fails to quantify the entanglement between the two subsystems. In such cases one can use negativity as a pertinent measure of entanglement, defined as [35, 36]

$$E = -1 + \sum_k |\eta_k| = 2 \sum_{\eta_k < 0} |\eta_k|, \quad (\text{S1})$$

where the η_k 's are the eigenvalues of the matrix $\rho_{AB}^{T_A}$ (or $\rho_{AB}^{T_B}$) in which T_A (or T_B) stands for partial transpose with respect to the subsystem A (or B). If the density matrix ρ_{AB} is separable, then both $\rho_{AB}^{T_A}$ and $\rho_{AB}^{T_B}$ remain positive and thus $\eta_k \geq 0$ for all k 's which results in zero negativity in Eq. (S1). In contrast, if the overall state ρ_{AB} is entangled then some of the η_k 's become negative and thus the negativity in Eq. (S1) becomes nonzero.

Negativity as a measure of entanglement, applicable for both pure and mixed states, is an entanglement monotone which means that it does not increase under local operations. Furthermore, negativity is a legitimate quantum mechanical observable in the sense that it is associated with a Hermitian operator as

$$\mathcal{O} = 2 \sum_{\eta_k < 0} (|\eta_k\rangle\langle\eta_k|)^{T_A}, \quad (\text{S2})$$

where $|\eta_k\rangle$'s are the eigenvectors of the matrix $\rho_{AB}^{T_A}$. So, one can easily show that $E = \text{Tr}(\rho_{AB}\mathcal{O})$.

2. Spin-chain representation of the 2CK model

The spin-chain representation of the spin sector of the two-channel Kondo model was first introduced in Ref. [11, 12]. To further justify this representation, we here provide a conformal field theory analysis.

By folding the system in half, creating an open boundary at the impurity site $l = 0$, the left and right parts of the spin chain come to define two "channels" on the interval $[0, Na/2]$, where a is the lattice spacing. Introducing slowly varying left/right-moving $\text{SU}(2)_1$ spin currents $\mathbf{J}_{LM/RM}^{(m)}$, together with two $\text{SU}(2)_1$ Wess-Zumino-Witten matrix fields \mathbf{g}^m [57], the representation

$$\sigma_l^{(m)} \rightarrow \mathbf{J}_{LM}^{(m)}(al) + \mathbf{J}_{RM}^{(m)}(al) + (-1)^l \text{Tr}(\mathbf{g}^{(m)}(al)\sigma), \quad (\text{S3})$$

can then be used in the continuum limit to map the folded $\Gamma = 1$ system onto the spin sector of the two-channel Kondo model [11, 12]. Since the two channels (a.k.a. spin chains) both couple to the impurity, the expected chiral $\text{SU}(2)_1 \otimes \text{SU}(2)_1$ symmetry of the critical theory in absence of the impurity gets replaced by $\text{SU}(2)_2 \otimes \mathbb{Z}_2$, where the Ising symmetry group \mathbb{Z}_2 encodes the presence of the two channels. This conformal embedding is different from the one used for the original two-channel Kondo model [5], and reflects the fact that the two underlying bulk theories are different: In the two-channel Kondo model one is dealing with non-interacting electrons with two orbital channels, whereas in its spin-chain representation the impurity host is that of a one-dimensional half-filled Hubbard model (with charge gapped out) and with only a single orbital. The Ising \mathbb{Z}_2 sector comes into play only off the two-channel Kondo critical point, and then contributes a leading scaling operator of the same dimension as that from the "flavor" sector in the conformal embedding used for the two-channel Kondo model [5]. This testifies to the consistency of the spin chain representation. Note that the total central charge implied by the spin-chain representation on a half-line, $c = c_{\text{SU}(2)} + c_{\text{Ising}} = 3/2 + 1/2 = 2$, becomes halved, $c = 1$, when doubling the spatial degrees of freedom by unfolding the system back to the full interval $[-Na/2, Na/2]$. The unfolded geometry is the one used in our DMRG computations, cf. Fig. 1.

3. Use of periodic boundary conditions in Fig 2

In most studies of the 2CK model there is no interaction between the two channels; however, for the results presented in Fig 2 the two channels are coupled through the periodic boundary conditions. For the remainder of the results presented this is not the case. As long as $x \ll N/2$ this should not affect the results for large enough N since in the limit $N \rightarrow \infty$ results have to be independent of this boundary condition. Obviously, once x approaches $N/2$ there is no reason to expect that we should correctly represent 2CK physics. This can for instance be seen in the inset of Fig. 2(b) where $S_{\text{imp}}(x, N)$ does not approach $\ln(2)/2$ as x approaches $N/2$. It is then reasonable to ask why we use periodic boundary conditions since numerically it would be simpler to use open boundary conditions. The *major* reason for this is that the correction to scaling terms appearing in Eq. (9), proportional to α , are well understood [45]. These terms are more correctly seen as arising from 1CK physics associated with the open boundary in the left panel of Fig. 2(b). In the presence of open boundary conditions several other terms would appear dominating the 2CK physics we are trying to study and it is therefore a significant advantage to employ the periodic boundary conditions as was done in Fig. 2. Furthermore, we note that H_{PBC} as defined in Eq. (2) approach a completely uniform chain in the limit $J' \rightarrow 1$ which is another advantage when extracting S_{imp} . For the results presented in Figs. 3,4 the above advantages of using H_{PBC} are not pertinent and we have therefore used the more standard H_{OBC} .

4. Limiting Behavior of S_{imp} as $J' \rightarrow 1$

As discussed in the main text $S_{\text{imp}}(J' \rightarrow 1) = \ln(2) - \ln(g_{UV}/g_{IR})$ using Eq. (4) and (7). This relation takes the view point of 2CK physics. It is of course also possible to remain with a purely spin-chain view point in which case it follows from Eq. (4) and (6) that $S_{\text{imp}}(J' \sim 1, x, N) \sim -2 \ln g = \ln(2)/2$ for $1 \ll x \ll N$. These two results just re-express the basic relation

$$g_{UV}/g_{IR} = 2g^2, \quad (\text{S4})$$

discussed in detail in the main text.